Microstructure and tribological properties of laser in-situ synthesized Ti_3Al composite coating on Ti-6Al-4V

Wenbin Zhang [a], Wensheng Li [a,*], Haimin Zhai [a], Yanrong Wu [b], Shuncai Wang [c], Gang Liang [b], Robert J K Wood [c]

a State Key Laboratory of Advanced Processing and Recycling of Nonferrous Metals, Lanzhou University of Technology, Lanzhou 730050, PR China

b Dongfang Electric Corporation Dongfang Turbine Co., Ltd, Deyang 618000, PR China

c National Centre for Advanced Tribology, Faculty of Engineering and the Environment, University of Southampton, Southampton, SO17 1BJ, United Kingdom

Abstract

Titanium intermetallics are highly significant to protect surfaces of lightweight structures against corrosion and wear. In this study, Ti and Al powders were uniformly mixed with an atomic ratio 65:35 and in-situ synthesized on the Ti-6Al-4V substrate by laser cladding with Ar cooling. The microstructure and high temperature tribological behavior were studied. The results show that Ti_3Al (α_2) phase was first precipitated in the form of coarse primary dendrites during cladding solidification, and subsequently α-Ti (α) phase of needle-shaped martensite was formed by fast cooling. The 6:4 ratio of phase α_2 to α of the composite coating provides optimal toughness and high hardness (680 HV). Under the testing up to 500 ℃, the average friction coefficients of the composite coatings range from 0.22 to 0.37 and a 35% lower wear rate than that of the Ti-6Al-4V substrate.

Key words: Ti_3Al composite coating; Laser cladding; Microstructure; Friction and Wear

1. Introduction

Due to the low density, high specific strength, excellent corrosion resistance and weldability, Ti-

*Corresponding author:
E-mail address: liws@lut.edu.cn (Wensheng Li)

6Al-4V alloy is one of the most important materials used for lightweight structure in the aviation, marine, petrochemical and automotive industries [1-3]. However, its low resistance to wear and oxidation at medium and high temperatures prevent the wide applications to engineering tribological components [4]. In contrast, Ti_3Al intermetallic compound (IMC), an ordered hexagonal structure of $D0_{19}$, has relatively high yield strength, creep and oxidation resistance at elevated temperatures [5,6]. Therefore, Ti_3Al coated on the surface of titanium alloy will significantly improve the latter's friction resistance of high temperature [7]. In recent years, the wear behaviour of Ti_3Al IMCs has been extensively studied [8-12]. Under the same dry sliding test conditions, the wear resistance of the hexagonal α_2-Ti_3Al is superior to the tetragonal intermetallic γ-TiAl which is commonly found in Ti-Al alloys [13]. An extra twinning in the cast Ti_3Al single crystals is seen exclusively at temperatures over 1000 °C when the compression axis is along or near the *c*-axis [14]. In the two-phase α_2 (Ti_3Al) + γ (TiAl) alloys, an addition of Nb was found to enhance twinning and reduce the antiphase domain boundary (APB) energy [15]. However, the use of a large quantity Nb is not economical due to its expense. At high temperatures, the oxidation of Al to Al_2O_3 prevents the penetration of oxygen into the alloy and maintains its high strength and good oxidation resistance [16]. However, due to the brittle spalling and poor toughness, Ti_3Al IMCs are rarely used for coatings of titanium alloys [17]. This research, therefore, focusses on the Ti and Al composition and phase ratio of the Ti_3Al composite coating to optimize its plasticity and brittleness and to further improve the high temperature wear resistance.

In-situ synthesis by laser cladding has become an excellent approach to prepare titanium alloy coatings because it produces good compactness, low dilution rate, high bonding strength, small heat-affected zone and fine grain size [18,19]. In this work, a two-phase composite coating containing α_2

and α was synthesized in-situ by laser cladding. Ar cooling was introduced to minimize the brittle fracture of Ti_3Al. The microstructure of the composite coating and its tribological behavior at evaluated temperature (25 ~ 500 ℃) were studied to provide guidance for surface protection and repair of titanium alloy components.

2. Experiments

2.1. Raw materials and cladding process

Ti-6Al-4V alloy with a size of 100 mm × 100 mm × 10 mm was used as the substrate. The chemical components are 5.0-6.5% Al, 3.5-4.5% V, 0.186% Fe, 0.019% Si, 0.05% O (in weight) with the remainder Ti. The substrate was mechanically polished and washed with acetone to remove oxides and oil stains on surface. Ti powder (particle size 50-74 μm, purity 99 %) and Al powder (particle size 74-150 μm, purity 99 %) were mixed to get a composition of 65 at. % Ti and 35 at. % Al and bonded to the surface of the substrate with 5 wt. % polyvinyl alcohol. Moisture in the adhesive layer was removed naturally for 24 h.

The fiber laser (YLS-4000, IPG, Germany) was employed with the maximum power output of 4000 W and the wavelength of 1.07 μm. The position accuracy of the six-axis linkage robot is 0.1 mm (KR500 R2830, KUKA, Germany). The experimental parameters include: 0 defocusing, 3 mm of spot diameter, 5 mm of the distance between the nozzle and substrate, the spot energy in Gaussian distribution, and an Ar coaxial feeding nozzle was used to cool and protect the molten pool from oxidization. The uniform coating without cracks and pores was obtained using laser power 1400 W, scanning velocity10 mm/s, and Ar flow 15 L/min. The laser scanning overlap rate of the coating used in the friction test was 40%. The coated samples were cut by wire cutting perpendicular to the direction of laser scanning.

2.2. Microstructure characterization and friction test

The metallographic structure was observed after etching with 5 ml HF + 5 ml HNO_3 + 90 ml H_2O solution for 10 ~ 15 s. The phase composition of the cladding composite coatings was analyzed by X-Ray diffraction (XRD, D8 Discover, Bruker) in the $2\theta = 10 \sim 90°$ (40 kV, 40 mA, Cu Kα radiation). Microstructure and surface morphology of the composite coatings after friction test were observed by field emission scanning electron microscope (SEM, Quanta 450FEG, FEI). The element distribution was analyzed by SEM equipped with energy dispersive spectrometer (EDS, AztecX-Max80, Oxford). The crystallographic orientation test was evaluated using an attached electron backscatter diffraction (EBSD, HKL Nordly, Oxford) instrument (acceleration voltage of 20 kV, step size 0.5 μm), and the data was processed by Channel 5 software. The EBSD Specimen was electrolytic polished by 6% perchloric acid + 34% butanol + 60% methanol solution at -30 ℃. Differential Scanning Calorimetry (DSC) analysis was performed on the mixed powders of Ti and Al under a protective atmosphere of Ar in a synchronous thermal analyzer (STA PT 1600, LINSEIS). The test temperature was 30 ~ 1500 °C and the heating rate was 5 °C/min. The nanoindenter (Agilent G200, USA) was used to obtain the mechanical properties of individual phases. The loading and unloading rates were 0.15 mN/s, with a dwell times of 2 s at the maximum loading force. Additionally, in order to obtain overall hardness and estimate the plastic toughness class of composite coatings, Vickers micro-hardness tester (HV-1000, China) was also performed on the polished cross section of the coatings with a load of 500 g, and the load was held for 10 s. Hardness values were obtained from at least 30 indentations. The toughness estimation criteria for acceptability were: (1) all cracks emanated from the corners, (2) presence of only four radial cracks, (3) no crack chipping and (4) no crack branching [20].

The tribological properties of the composite coating were tested using a HT-1000 pin-disk high-

temperature friction tester (Zhong Ke Kai Hua Corporation, China) at a heating rate of 10 °C/min. The disk (ø 20 × 5 mm) cladded by the composite coating was used. The sliding counterpart was a SiC ball (ø 6 mm, hardness > 1300 HV, compressive strength 2200 MPa and high temperature resistance 1000°C). The test temperatures were respectively 25 °C, 100 °C, 300 °C, 500 °C, respectively. The rotating line speed of the disk is 10 mm/s, the load of 5 N, and the sliding duration of 30 min. The wear volume was measured using an MT-500 Probe type two-dimensional profiler (Zhong Ke Kai Hua Corporation, China).

3. Results and discussion

3.1. Microstructure and mechanical properties of Ti_3Al composite coating

Fig. 1 shows SEM images viewed on cross-section of the composite coating. After laser scanning, the composite coating surface is smooth and uniform without pores. The thickness of the composite coating is about 550 μm. In general, the composite coating is composed of fine needle-like structures, that is, a martensitic-like structure formed by rapid cooling of the molten pool. The convex white line inside the composite coating is the area of the enriched α_2 (Ti_3Al) phase [21]. The smooth transition layer shows the uniform interface between the substrate and coating (Fig. 1(c)).

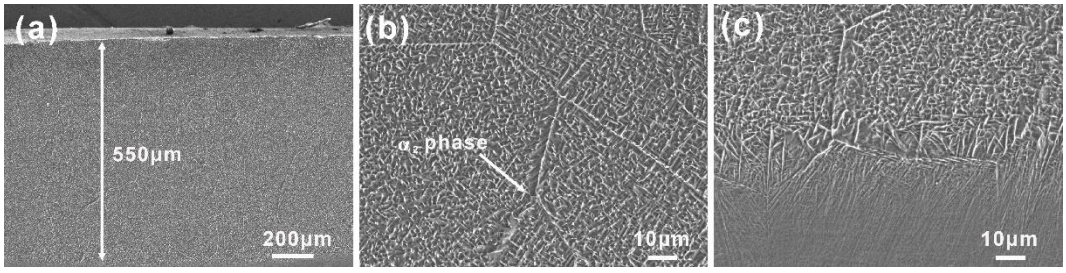

Fig. 1. SEM images of the cross-section of composite coating: (a) low magnification, (b) high magnification, (c) interface between coating and substrate.

Fig. 2(a) shows the XRD pattern of the composite coating which confirms the existence of both α_2 phase and α phase. Fig. 2(b) is the hardness profile of the cross-section as a function of the distance

away from the composite coating surface. The hardness of the substrate is about 370 HV which is much lower than the composite coating (680 HV). Fig. 2(c) represents the load-displacement curves of Ti_3Al phase and α-Ti phase obtained by the nanoindentation testing. The indentation plastic P of the composite coating was evaluated according to [22]: $P = \frac{AB}{AC}$, where AB is the residual depth, and AC is the indentation depth. The P values for Ti_3Al and α-Ti are 0.696 and 0.804 respectively, which indicates that the plastic deformation ability of Ti_3Al phase is smaller than α-Ti phase. The mechanical properties of Ti_3Al phase and α-Ti are summarized in Table 1. It also shows that the Ti_3Al exhibits a high nanohardness of about 7.62 GPa, which is about 3.8 times that of α-Ti (2.02 GPa). Generally, in terms of elasticity and failure behavior, the ratio of hardness (H) divided by elastic modulus (Er) (H/Er) is the factor for determining the elastic limit in surface contact. In terms of yield behavior, (H^3/Er^2) is an important parameter to describe the material's resistance to plastic deformation under load contact [23]. With both the highest H^3/Er^2 (1.914×10^{-2}) and H/Er (0.051) of the Ti_3Al IMCs, the composite coating presents much higher hardness, compressive strength and plastic deformation ability than that of the Ti-6Al-4V substrate.

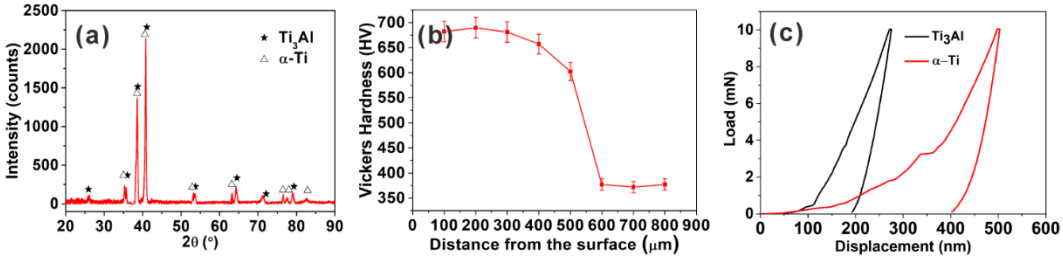

Fig. 2. (a) XRD pattern of composite coating, (b) microhardness of composite coating, (c) load vs. displacement curves for Ti_3Al and α-Ti.

Table 1 Mechanical properties of Ti_3Al phase and α-Ti phase after nanoindentation. elastic modulus (Er), nanoindentation hardness (H), vickers microhardness (HV), maximum displacement depth (h_m), H/Er and H^3/Er^2 value.

Phase	*Er* (GPa)	*H* (GPa)	HV	h_m (nm)	*H/Er*	H^3/Er^2

Ti_3Al	152.079	7.621	705.819	503.249	0.050	1.914×10^{-2}
α-Ti	82.089	2.022	187.273	275.389	0.025	1.226×10^{-3}

In order to understand the solidification of Ti-Al IMCs in laser cladding molten pool, the mixed powder was analyzed by DSC as shown in Fig. 3. Two significant endothermic peaks appear near 653 °C and 1376 °C, and one exothermic peak appears near 762 °C. Since the molten point of pure Al is 653 °C [24], the first endothermic peak should correspond to the melting point of Al powder. With the increasing of temperature, Al powders were melted and fully cover the surface of Ti powders. When the temperature reaches to 762 °C, the molten Al reacted with Ti powders to form the γ (TiAl) phase [25], which corresponded to the first exothermic peak of 762 °C in DSC curve. The second endothermic peak at 1376 °C corresponded to the formation of α_2 phase by a peritectic reaction [26]. Since the Al atoms have high diffusion activation energy at elevated temperatures, their diffusion is localized to form Al-rich IMC [27]. Correspondingly, during the laser cladding process, attributed to high energy density of the laser cladding, the mixed Al and Ti powder super-fast melted and then changed to liquid state into the molten pool on the Ti-6Al-4V substrate. Under the high-speed cooling of inert Ar gas, the Ti_3Al phase is formed first and then quickly grows to form primary coarsening dendrites with a size of several micrometers (Fig. 2(a)), the remaining Ti solidified as α phases with a size of several tens of micrometers (Fig. 1(b)).

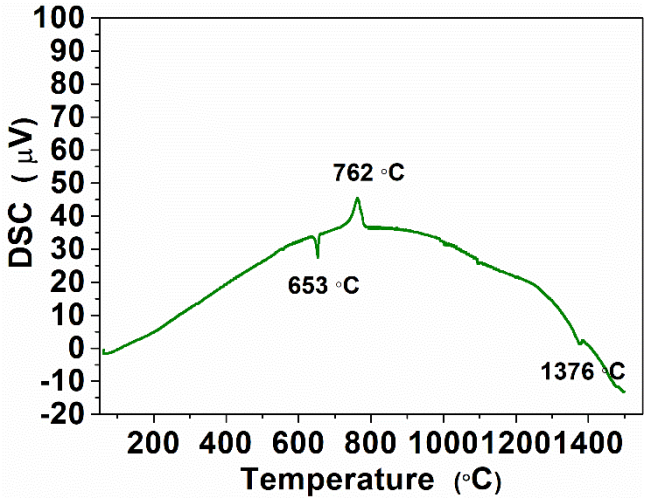

Fig. 3. DSC curve of Ti and Al mixed powders.

3.2. EBSD analysis of the Ti_3Al composite coating

Fig. 4 shows the EBSD pattern near the composite coating surface. Fig. 4(a) is the diffraction back scattered electron (BSE) pattern. The contrast of BSE pattern is relates to the average atomic number so the shallow white areas are Ti-Al IMCs. The EBSD phase contrast in Fig. 4(b) confirms the blue and yellow regions corresponding to α_2 phase and α phase, respectively. According to Channel 5 software statistics, α_2 phase accounts for 57.8%, α phase accounts for 41.2%, and TiAl (γ) phase for 1%. The ratio of α_2 phase to α phase is approximately 6:4, and the grain size distribution is shown in Fig. 4(c). The grains below 0.5 μm accounted for 65% within the selected area, and the remaining grains were all below 1 μm. The large grains are concentrated in the shallow white area of mainly α_2 phase. Fig. 4(d) shows the distribution of different structures in the selected area. The blue, yellow and red regions are recrystallization, substructure and deformed structures, respectively. According to Fig. 4(b), the substructure region is mainly α_2 phase, and the recrystallization and the deformed structure mainly occur in α phase. The components of the three structures are 38.11%, 41.47%, and 20.42%, respectively. Fig. 4(e) shows grain shape and grain boundary types of the composite coating. The grain boundary with the difference orientation of 2 ~ 15° is defined as the low-angle grain boundary, and the

grain boundary of higher than 15° is the high-angle grain boundary [28]. It can be seen that the difference in grain orientation distribution in the left and right is clearly divided by of the white line (Fig. 4(e)); and the count for the high-angle grain boundary and low-angle grain boundary is about 69.7% and 30.3%, respectively, as shown in Fig. 4(f). The grains appear in the cast dendritic structure with two primary trunks in large orientation difference. The primary dendrite and the need-like secondary dendrites have different sizes but not orientation, Fig. 4(g) shows the misorientation angle distribution of two phases. The orientation distribution of the two phases is not distinguishable, indicating the presence of texture in the coating. It can be accounted that the ratio of α_2 phase to α phase is about 6: 4. Through the Vickers micro-hardness measurements of the composite coatings, the coating shows adequate plastic toughness as there are no cracks branching from the corner of the Vickers indent. This part has been detailed in the experimental part of section 2.2.

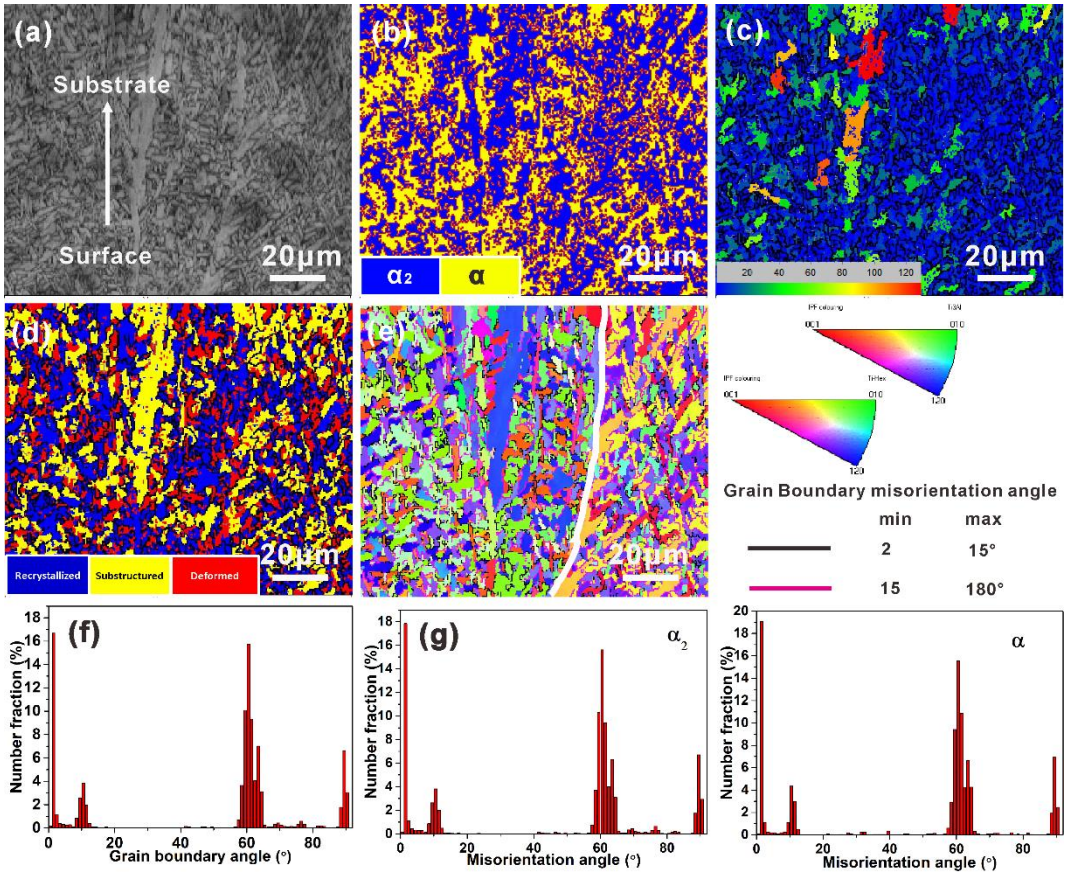

Fig. 4. Electron backscattered pattern of the coating near surface: (a) back scattered electron (BSE) pattern, (b) phase

distribution, (c) grain size distribution, (d) crystallization distribution, (e) grains and boundaries types, (f) grain boundary angle distribution, (g) misorientation angle distribution.

The grain size and grain distribution of the composite coating are closely related to the laser heat loss. Argon, acted as a protective and cooling gas homogenously [29], will not be involved into the chemical reaction process during the circulating flow in the molten pool [30]. Rapid solidification results in the fine needle-like (martensite-like) structure in the composite coating (Fig. 1 and Fig. 4(a)). The dendritic trunks on both sides are not parallel to each other (Fig. 4(e)). From the distribution of phases and EBSD analytical result, the primary and secondary dendrimers were α_2 phase, and the interval between the dendrites should be α phase. Since the α_2 phase is formed first during solidification, α phase is nucleated and grows at the α_2 phase substructure boundary (Fig. 4(b) and 4(f)). The two phases have basically the same microstructure orientation distribution (Fig. 4(e)).

As shown in the DSC result (Fig. 3), Ti and Al powders were rapidly heated to a liquid state by laser cladding with sufficient diffusion. During the Ar super cooling solidification, Ti_3Al (α_2) phase firstly precipitated in the form of coarse primary dendrites, the remained Ti formed the needle-shaped martensiticα-Ti (α) in rapid sequence, but the content of TiAl (γ) phase in the coating is very small (only accounts for 1%). All the formed grains are relatively small, and most of them are about 0.5 μm in size (Fig. 4(c)).

3.3 Tribological behavior of the Ti-6Al-4V substrate and Ti_3Al composite coating

Fig. 5 shows the friction coefficient curves of Ti-6Al-4V substrate and the composite coating at different temperatures (25 ~ 500 °C). At individual temperatures, the friction coefficients of the uncoated Ti-6Al-4V substrate versus sliding time curves quickly stabilize and remain constant. With the increase of temperature from 25 °C to 500°C, the average friction coefficients gradually decrease

from 0.30 ± 0.015 to 0.20 ± 0.010 (Fig. 5(a)). Unlike the Ti-6Al-4V substrate, the friction coefficients of the composite coating versus sliding time curves show fluctuations, in which with the increase of temperatures, the fluctuation becomes more evident as shown in Fig. 5(b). Similar to the Ti-6Al-4V substrate, the average friction coefficients gradually decrease from 0.37 ± 0.018 to 0.22 ± 0.011 when the temperature increases from 25 °C to 500°C.

Fig. 6 shows the wear rate of Ti-6Al-4V substrate and composite coating at different temperatures (25 ~ 500 °C). When the temperature increased from 25 °C to 100 °C, the wear rates of Ti-6Al-4V substrate reduced significantly from 7.67 × 10^{-3} mm^3/Nm to 3.06 × 10^{-3} mm^3/Nm. With further increases in temperature to 300 °C and 500 °C, the wear rates decrease gradually to 1.97 × 10^{-3} mm^3/Nm and 1.83 × 10^{-3} mm^3/Nm, respectively. In contrast, from 25 °C to 300 °C, the wear rates of the composite coating change slightly from 4.06 × 10^{-3} mm^3/Nm to 3.25 × 10^{-3} mm^3/Nm. When the temperature increases to 500 °C, the wear rates of the composite coating rapidly dropped to 1.36 × 10^{-3} mm^3/Nm.

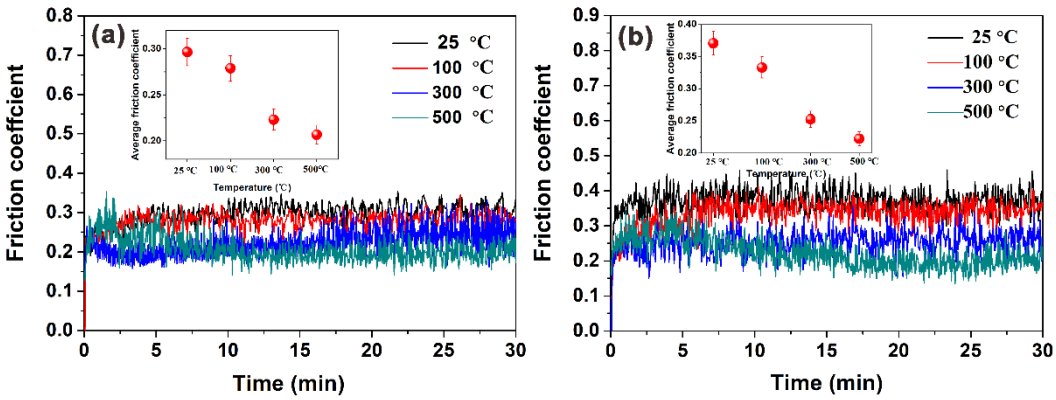

Fig. 5. Friction coefficient curves at different temperatures: (a) substrate, (b) coating.

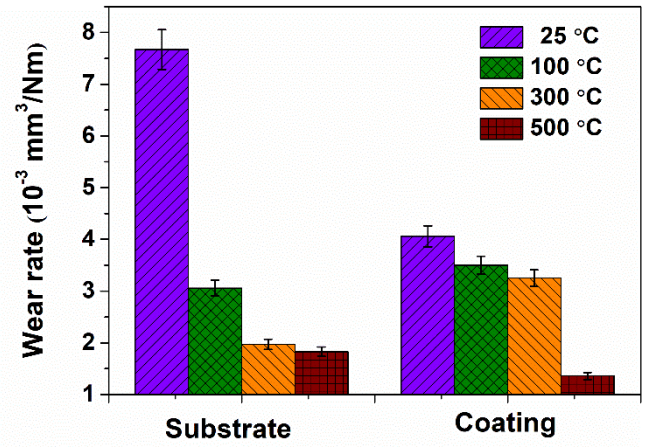

Fig. 6. Wear rate at different temperature.

Fig. 7 and 8 show the worn surface morphologies and 2-dimensional (2D) profiles of wear tracks of the composite coating and the counterpart in a range of temperatures (25 ~ 500 °C), respectively. Both the furrow's width and depth on the worn surface of the Ti-6Al-4V substrate and the composite coating gradually reduced with the increasing temperature between 25 °C to 500 °C (Fig. 7), which is consistent with the evolution of the wear rate in Fig. 6. Moreover, the corresponding worn surface area of the counterpart also gradually decreased with the increasing temperature between 25 °C to 500 °C (Fig. 8).

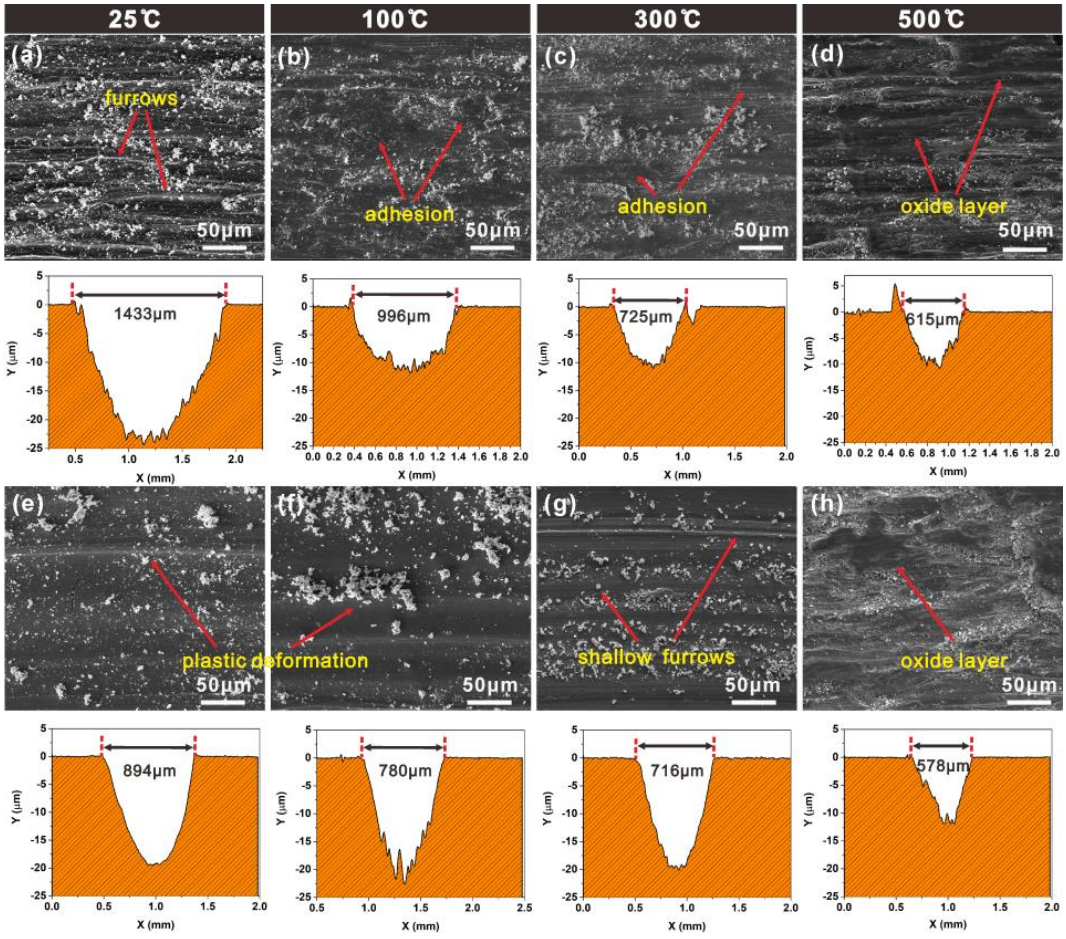

Fig. 7. Wear morphologies and 2-dimensional (2D) profiles of wear tracks at different temperatures: (a)-(d) Ti-6Al-4V substrate, (e)-(h) coating.

For the Ti-6Al-4V substrate, adhesive wear is dominant in the temperature range from 100 °C to 300 °C. The adhesion patches on the surface of the counterpart gradually increased which was accompanied by a decrease in worn area of the counterpart (Fig. 8(c)). When the temperature reaches to 500 °C, a continuous and smooth oxidation layer appears on the worn surface of Ti-6Al-4V substrate, indicating that the wear mechanism transfer from adhesive wear to oxidation wear (Fig. 7(d)). In contrast to Ti-6Al-4V substrate, much more severe deformed debris were distributed on the worn surface of the composite coatings from 25 °C to 100 °C (Fig. 7(e) and (f)). The adhered surfaces and transfer film are hardly observed in the image or detected by EDS. When the test temperature reaches to 500 °C, the worn surface of the composite coating generates numerous fine debris and a polished

oxidation film (Fig. 7(h)). This indicates that as the test temperature increased from 25 °C to 500 °C, the degree of plastic deformation of the composite coating gradually decreased and changed to oxidation wear.

3.4 Tribological mechanism of Ti_3Al composite coating

From the Figs. 5-8, it can be deduced that the composite coating has excellent wear resistance compared with the Ti-6Al-4V substrate. This is attributed to the high hardness, compressive strength and toughness of the composite coating for the ratio of α_2 and α phase to 6:4 in the composite coating.

During the friction and wear process at 25 °C, the Ti-6Al-4V substrate direct contacts with the high hardness SiC ball counterpart (over than 1300 HV), which causes severe plastic deformation on the substrate surface. This results in deep furrows, large debris and high wear rate, as shown in Fig. 6-8. Moreover, the severe wear leads to abundant debris adhered to the counterpart surface, resulting in an uneven surface in the counterpart surface (Fig. 8(a)) and relatively high friction coefficient (0.30 ± 0.015) (Fig. 5(a)). When the test temperatures are over than 100 °C, the dislocation annihilation rates in the Ti-6Al-4V titanium alloy begin faster than their formation rate [31], which leads to the softening of the substrate. Besides, as the test temperature increased, the oxide film gradually appeared on the worn surface of the Ti-6Al-4V substrate (Fig. 7(a)-(d) and Fig. 9). This leads to a self-lubricating effect [32], so the friction coefficient and wear of the substrate gradually decrease with increasing test temperature. Especially in the 500 °C, the oxygen content inside of the worn surface increased to 44 at. % (Fig. 9) corresponding to an smooth oxidation layer on the worn surface (Fig. 7). Therefore, the friction coefficient at 500 °C was dropped significantly to 0.20 ± 0.010 (Fig. 5).

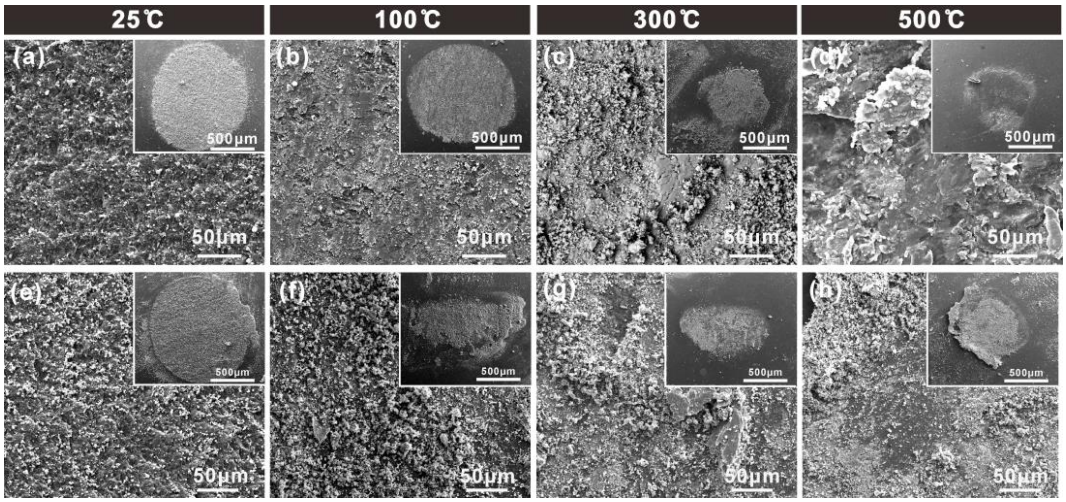

Fig. 8. Surface morphologies of counterpart against Ti-6Al-4V substrate and composite coating: (a)-(d) Ti-6Al-4V substrate, (e)-(h) coating.

The laser cladding coating composed of hard α_2 (705.8 HV) and soft α phase (187.3 HV) (Fig. 4(b) and Table 1) show uniform structure and are pore free (Fig. 1). Inside the composite coating, the α_2 phase acts as framework support, whereas α phase acts as a medium to connect with hard α_2 phase [17]. By control of α_2 and α phase ratio to 6:4, the composite coating shows high hardness (680 HV), increased compressive strength and adequate toughness. Hence, the microconvex depth of the worn surface on the composite coating is relatively shallow and no microcracks appear on the surface (Fig. 7 (e)-(g) and Fig. 8(e)-(g)). When friction and wear test performed at low temperature (25 ~ 300 °C), there is only 1/6 <1120> dislocation inside α_2 phase can participate in plastic deformation (Fig. 4) and the <0001> dislocation is almost absent, which leads to the brittle cleavage and poor plasticity [33, 34]. The surface of the worn morphologies show limited adhesion, i.e. the large and hard debris have been peeled off from the worn surface (Fig. 7(e)-(g)). Therefore, the hard debris between the counterpart surface and composite coating surface lead to the formation of furrows on the worn surface, corresponding to unstable friction processes, high coefficients of friction (Fig. 5b) and high wear rate at low temperature (25 ~ 300 °C) (Fig. 6). When the test temperature increases to 500 °C, the Ti_3Al

grain boundary relaxation activity is increased and accompanied by a decreasing in the strength of the coating [35], as confirmed by the adhesion and transfer film on the worn surface (Fig. 7 (h)). Besides, the high test temperature also leads to form the oxidation tribofilm (oxygen content on the counterpart worn surface is about 26.8 at. %). This enhances the lubrication effect of the coating [32], and results in a decrease of the friction coefficient and wear rate (Fig. 5(b) and Fig. 6). Compared to the Ti-6Al-4V substrate, the composite coating had a gradual decrease of oxygen content with the temperature increase from 25 °C to 500 °C. With the increase of testing temperature, the oxidation of the composite coating is less critical than that of Ti-6Al-4V substrate (Fig. 9), thus the wear rate of the composite coating is lower, relatively, than that of the Ti-6Al-4V substrate at the high temperature, i.e. the composite coating can provide better protection against wear and oxidation to the Ti-6Al-4V substrate at the evaluate test temperature range (25 °C to 500 °C), especially in the high temperature (500 °C).

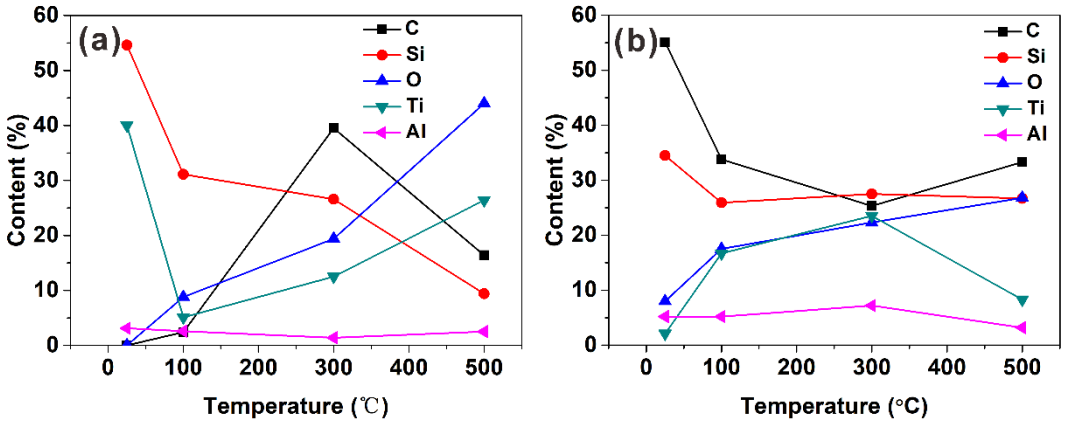

Fig. 9. Surface element content distribution of counterpart surface after wear test at different temperatures: (a) substrate, (b) coating.

4. Conclusions

A composite coating of α_2 (Ti_3Al) and α (Ti) has been synthesized in-situ by laser cladding process on the surface of Ti-6Al-4V substrate with Ar cooling. The tribological behavior of coating was studied between the temperatures of 25 °C to 500 °C. The main findings are summarized as follows:

1. During the laser cladding on Ti and Al mixed powders solidification with Ar cooling, α_2 phase firstly formed as coarse primary dendrites, followed by α phase nucleus and growth, in the form of acicular martensite structure. The composite coating is mainly composed of Ti_3Al (α_2) and α-Ti (α) phases with the minority of TiAl (γ) phase content less than 1%.

2. Ti_3Al phase (α_2) has high H^3/E^2 (1.914×10^{-2}) and H/E (0.051) values, while α-Ti phase (α) has a lower H^3/E^2 (1.226×10^{-3}) and H/E (0.025) values. The 6:4 ratio of α_2 and α phase of composite coating provide an adequate toughness and the hardness (680 HV).

3. During the friction process and wear process (25 ~ 500 ℃), no brittle peeling occurred on the worn surface of the composite coating due to its adequate toughness. The high hardness and high temperature oxidation resistance of the Ti_3Al composite coating resulted in a 35% lower wear rate (1.36×10^{-3} mm^3/Nm) than that of Ti-6Al-4V substrate (1.83×10^{-3} mm^3/Nm).

Acknowledgments

The authors would like to acknowledge the support of National Natural Science Foundation of China (No. 51674130), International Science and Technology Cooperation Program of China (2015DFR51090), the National High-end Foreign Experts Program of China (GDT20186200331), the International Science and Technology Correspondent Program of Gansu Province (17JR7WA017), and the program of "Science and Technology International Cooperation Demonstrative Base of Metal Surface Engineering along the Silk Road".

References

[1] R.R. Boyer, An overview on the use of titanium in the aerospace industry, Mater. Sci. Eng. A 213 (1996) 103-114.

[2] Y.S. Tian, C.Z. Chen, S.T. Li, Q.H. Huo, Research progress on laser surface modification of titanium alloys, Appl. Surf. Sci. 242 (2005) 177-184.

[3] H.M. Zhai, H.F. Wang, F. Liu, A strategy for designing bulk metallic glass composites with excellent work-hardening and large tensile ductility, J. Alloy. Comp. 685 (2016) 322-330.

[4] M. Peters, J. Kumpfert, C.H. Ward, C. Leyens, Titanium Alloys for Aerospace Applications, Adv. Eng. Mater. 5 (6) (2003) 419-427.

[5] S. Djanarthany, J.-C. Viala, J. Bouix, An overview of monolithic titanium aluminides based on Ti_3Al and TiAl, Mater. Chem. Phys. 72 (2001) 301-319.

[6] S.Y. Lyu, Y.B. Sun, L. Ren, W.L. Xiao, C.L. Ma, Simultaneously achieving high tensile strength and fracture toughness of Ti/Ti-Al multilayered composites, Intermetallics 90 (2017) 16-22.

[7] H.X. Liu, X.W. Zhang, Y.H. Jiang, R. Zhou, Microstructure and high temperature oxidation resistance of in-situ synthesized TiN/Ti_3Al intermetallic composite coatings on Ti6Al4V alloy by laser cladding process, J. Alloy. Comp. 670 (2016) 268-274.

[8] H. Lee, H. Kang, J. Kim, H.-K. Shin, J. Lee, S.-H. Huh, J. Sung, H.-J. Lee, Inward diffusion of Al and Ti_3Al compound formation in the Ti-6Al-4V alloy during high temperature gas nitriding, Sur. Coat. Tech. 240 (2014) 221-225.

[9] J.N. Li, C.Z. Chen, T. Squartini, Q.S. He, A study on wear resistance and microcrack of the Ti_3Al/TiAl+TiC ceramic layer deposited by laser cladding on Ti-6Al-4V alloy, Appl.Surf. Sci. 257 (2010) 1550-1555.

[10] K. Zhang, T.B. Zhang, X.H. Zhang, L. Song, Corrosion resistance and interfacial morphologies of a high Nb-containing TiAl alloy with and without thermal barrier coatings in molten salts, Corros. Sci. 156 (2019) 139-146.

[11] B. Shao, D.B. Shan, B. Guo, Y.Y. Zong, Plastic deformation mechanism and interaction of B2, α_2, and O phases in Ti-22Al-25Nb alloy at room temperature, Int. J. Plasticity 113 (2019) 18-34.

[12] L. Cheng, J.S. Li, X.Y. Xue, B. Tang, H.C. Kou, O. Perroud, E. Bouzy, Effect of β/B2 phase on cavitation behavior during superplastic deformation of TiAl alloys, J. Alloy. Comp. 693 (2017) 749-759.

[13] B.G. Guo, J.S. Zhou, S.T. Zhang, H.D Zhou, Y.P. Pu, J.M. Chen, Tribological properties of titanium aluminides coatings produced on pure Ti by laser surface alloying, Sur. Coat. Tech. 202 (2008) 4121-4129.

[14] K. Kishida, Y. Takahama, H. Inui, Deformation twinning in single crystals of a $D0_{19}$ compound with an off-stoichiometric composition (Ti–36.5at.%Al), Acta Mater. 52 (2004) 4941-4952.

[15] L. Song, L. Wang, M. Oehring, X.G. Hu, F. Appel, U. Lorenz, F. Pyczak, T.B. Zhang, Evidence for deformation twinning of the $D0_{19}$-α_2 phase in a high Nb containing TiAl alloy, Intermetallics 109 (2019) 91-96.

[16] V. Maurice, G. Despert, S. Zanna. P. Josso, M.-P. Bacos, P. Marcus, XPS study of the initial stages of oxidation of α_2-Ti_3Al and γ-TiAl intermetallic alloys, Acta Mater. 55 (2007) 3315-3325.

[17] H. Wu, G.H. Fan, L. Geng, X.P. Cui, M. Huang, Nanoscale origins of the oriented precipitation of Ti_3Al in Ti–Al systems, Scripta Mater. 125 (2016) 34-38.

[18] Y.P. Kathuria, Some aspects of laser surface cladding in the turbine industry, Sur. Coat. Tech. 132 (2000) 262-269.

[19] C.T. Kwok, H.C. Man, F.T Cheng, K.H. Lo, Developments in laser-based surface engineering processes: with particular reference to protection against cavitation erosion, Sur. Coat. Tech.291 (2016) 189-204.

[20] E.A. Tsitrou, S.E. Northeast, R.V Noort, Brittleness index of machinable dental materials and its relation to the marginal chipping factor, J. Dent. 35 (2007) 897-902.

[21] B. Shao, S.X. Wan, W.C. Xu, D.B. Shan, B. Guo, Y.Y. Zong, Formation mechanism of an α_2 phase-rich layer on the surface of Ti-22Al-25Nb alloy, Mater. Charact. 145 (2018) 205-209.

[22] H. Guo, S.D. Zhang, W.H. Sun, J.Q. Wang, Differences in dry sliding wear behavior between HVAF-sprayed amorphous steel and crystalline stainless steel coatings, J. Mate. Sci. Technol. 35 (2019) 865-874.

[23] A. Matthews, A. Leyland, Material related aspects of nanostructured tribological coatings, SVC Bulletin 40 (2008) 40-45.

[24] J.-G. Luo, V.L. Acoff, Using cold roll bonding and annealing to process Ti/Al multi-layered composites from elemental foils, Mater. Sci. Eng. A 379 (2004) 164-172.

[25] R.K. Gupta, B. Pant, V. Agarwala, P.P. Sinha, Differential scanning calorimetry and reaction kinetics studies of $\gamma+\alpha_2$ Ti aluminide, Mater. Chem. Phys. 137 (2012) 483-492.

[26] M. Sujata, S. Bhargava, S. Sangal, On the formation of $TiAl_3$ during reaction between solid Ti and liquid Al, J. Mater. Sci. Lett. 16 (1997) 1175-1178.

[27] N. Bertolino, M. Monagheddu, A. Tacca, P. Giuliani, C. Zanotti, U.A. Tamburini, Ignition mechanism in combustion synthesis of Ti–Al and Ti–Ni systems, Intermetallics 11 (2003) 41-49.

[28] B.Y. Li, K.F. Zhang, W. Yao, B.T. Xu, Effects of current-assisted heat treatment time on microstructure evolution and superplastic properties of Ti-22Al-24Nb-0.5Mo alloy, Mater. Charact. 150 (2019) 38-51.

[29] M. Doubenskaia, A. Domashenkov, I. Smurov, P. Petrovskiy, Study of Selective Laser Melting of intermetallic TiAl powder using integral analysis, Int. J. Mach. Tool. Manu. 129 (2018) 1-14.

[30] T.R. Anthony, H.E. Cline, Surface rippling induced by surface-tension gradients during laser surface melting and alloying, J. Appl. Phys. 48 (1977) 3888-3894.

[31] W.-S. Lee, C.-F. Lin, Plastic deformation and fracture behaviour of Ti-6Al-4V alloy loaded with high strain rate under various temperatures, Mater. Sci. Eng. A 241 (1998) 48-59.

[32] A. Hirose, T. Ueda, K.F. Kobayashi, Wear and oxidation properties of titanium aluminides formed on titanium surface by laser alloying, Mater. Sci. Eng. A 160 (1993) 143-153.

[33] Y. Minonishi, M.H. Yoo, Anomalous temperature dependence of the yield stress of Ti_3Al by {1121} 〈1126〉 slip, Phil. Mag. Lett. 61 (4) (1990) 203-208.

[34] Y. Umakoshi, T. Nakano, T. Takenaka, K. Sumimoto, T. Yamane, Orientation and temperature dependence of yield stress and slip geometry of Ti_3Al and Ti_3Al-V single crystals, Acta Metall. Mater. 41 (4) (1993) 1149-1154.

[35] R.M. Imayev, N.K. Gabdullin, G.A. Salishchev, O.N. Senkov, V.M. Imayev, F.H. Froes, Effect of grain size and partial disordering on ductility of Ti_3Al in the temperature range of 20–600°C, Acta Mater. 47 (6) (1999) 1809-1821.